CHIN. PHYS. LETT. Vol. 37, No. 2 (2020) 027502

Physical Properties of Half-Heusler Antiferromagnet MnPtSn Single Crystal *

Qi Wang(王琦)[1], Qianheng Du(杜乾衡)[2], Cedomir Petrovic[2**], Hechang Lei(雷和畅)[1**]

[1]*Department of Physics and Beijing Key Laboratory of Opto-electronic Functional Materials & Micro-nano Devices, Renmin University of China, Beijing 100872*

[2]*Condensed Matter Physics and Materials Science Division, Brookhaven National Laboratory, Upton, New York 11973, USA*

(Received 5 December 2019)

We report the growth of ternary half-Heusler MnPtSn single crystals and detailed study on its structural and physical properties. MnPtSn single crystal has a larger lattice parameter than that in polycrystal and it exhibits antiferromagnetism with transition temperature T_N at about 215 K, distinctly different from the ferromagnetism of MnPtSn polycrystal. Hall resistivity measurement indicates that the dominant carriers are hole-type and the nearly temperature-independent carrier concentration reaches about 2.86×10^{22} cm^{-3} at 5 K. Moreover, the carrier mobility is also rather low ($4.7\,cm^2 \cdot V^{-1}s^{-1}$ at 5 K). The above results strongly suggest that the significant Mn/Sn anti-site defects, i.e., the content of Mn in MnPtSn single crystal, play a vital role on structural, magnetic and transport properties.

PACS: 75.50.Ee, 75.47.Np, 75.47.−m DOI: 10.1088/0256-307X/37/2/027502

Full-Heusler compounds X_2YZ and related half-Heusler compounds XYZ have attracted a great deal of attention due to the importance for basic science and potential application in spintronic devices.[1–6] Here, X and Y are transition metals or rare-earth elements and Z is a main group element. They show a variety of exotic phenomena, including metallic ferromagnetism, superconductivity, heavy fermion behavior, large magnetoresistance, and topological states, etc. Taking an example, many of full-Heusler compounds are ferromagnets, such as Cu_2MnAl, Cu_2MnSn, Ni_2MnSb, Ni_2MnSn.[7,8] More importantly, de Groot *et al.* first predicted that half-Heusler NiMnSb and PtMnSb are half-metallic ferromagnets (HMFMs).[9] In HMFMs, the band of minority spin electrons has a semiconducting gap at the Fermi energy level E_F, while the band of majority spin electrons is partially occupied. As a consequence, there is a 100% spin polarization of conduction electrons at the E_F. This is very important for spintronics. Since then, some of full-Heusler compounds have also been predicted to be HMFMs in theory[3,10–12] and later confirmed experimentally, such as Co_2MnSi.[13] When compared to ferromagnetic Heusler materials, antiferromagnetic (AFM) full- or half-Heusler compounds, such as CuMnSb,[8,14] Pt_2MnGa,[15] and RPtBi (R = Gd, Nd, Tb),[16–19] are relatively rare. However, they exhibit many of novel properties, like topological Weyl semimetal state in RPtBi.[18]

Among these materials, Mn-based Heusler compounds Mn_xPtSn show some interesting physical properties. Half-Heusler MnPtSn polycrystal is ferromagnetic (FM) with high Curie temperature $T_C \sim 330$ K and exhibits anomalous Hall effect (AHE).[20] Moreover, topological Hall effect has been observed in ferromagnetic Mn_xPtSn thin films ($x = 1.5$, 2),[21,22] and bulk materials ($x = 1.4$, 2).[23,24] In this work, we grew MnPtSn single crystals successfully. It is found that distinctly different from the FM MnPtSn polycrystal, MnPtSn single crystal shows an AFM ordering below 215 K. Such a difference possibly originates from the change of the atomic ratio in MnPtSn single crystal due to the existence of anti-site defects.

Experimental.—Single crystals of MnPtSn were grown by using Sn flux. Mn pieces (purity 99.99%), Pt pieces (purity 99.99%) and Sn granules (purity 99.99%) with a molar ratio of Mn : Pt : Sn = 3 : 2 : 30 were placed into an alumina crucible. The crucible was sealed in quartz ampoule under partial argon atmosphere. The sealed ampoule was heated up to 1373 K for 12 h and held for 8 h. Then it was cooled down to 973 K at a rate of 3 K/h. Finally, the ampoule was decanted with a centrifuge to separate MnPtSn crystals from excessive Sn flux at this temperature. X-ray diffraction (XRD) patterns were measured by using a Bruker D8 x-ray diffractometer with Cu K_α radiation ($\lambda = 0.15418$ nm) at room temperature. The elemental analysis was performed using inductively coupled plasma atomic emission spectroscopy (ICP-

*Supported by the National Key R&D Program of China (Grant Nos. 2018YFE0202600, 2016YFA0300504), the National Natural Science Foundation of China (Nos. 11574394, 11774423, 11822412), the Fundamental Research Funds for the Central Universities, the Research Funds of Renmin University of China (RUC) (Nos. 15XNLQ07, 18XNLG14, 19XNLG17), and the Office of Basic Energy Sciences, Materials Sciences and Engineering Division, U.S. Department of Energy (DOE) under Contract No. DE-SC0012704.

**Corresponding authors. Email: petrovic@bnl.gov; hlei@ruc.edu.cn

© 2020 Chinese Physical Society and IOP Publishing Ltd

AES). Magnetization, resistivity and thermal transport (TTO) measurements were carried out in Quantum Design PPMS. Longitudinal and Hall electrical resistivity data were measured simultaneously in a standard five-probe configuration. In order to effectively get rid of the influence of voltage probe misalignment, we measured the resistivity at positive and negative fields from 9 T to −9 T. The final longitudinal and Hall resistivity values were obtained by symmetrizing and antisymmetrizing raw data. TTO properties were measured using the four-probe method for the heat flow along the (111) plane and magnetic field applied along the [111] direction.

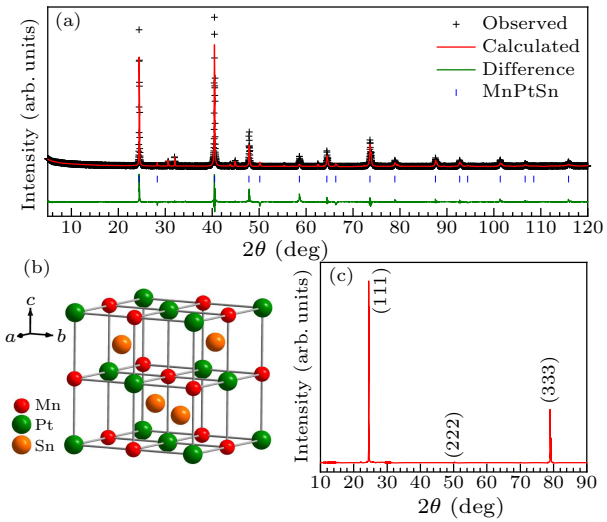

Fig. 1. (a) Powder XRD pattern and Rietveld refinement of ground MnPtSn single crystals. Vertical tickmarks denote Bragg reflections of the $F\bar{4}3m$ space group. (b) Crystal structure of MnPtSn. The red, green and orange balls represent Mn, Pt, Sn atoms, respectively. (c) XRD pattern of a MnPtSn single crystal.

Results and discussion.—The powder XRD pattern of ground MnPtSn single crystals is presented in Fig. 1(a). All peaks can be well indexed by the space group $F\bar{4}3m$ (No. 216), confirming that the obtained MnPtSn single crystal has a half-Heusler structure. Some peaks with negligible intensities are due to the minor second phase of Sn, coming from the residual flux on the surface of crystals. As shown in Fig. 1(b), MnPtSn with half-Heusler structure is composed of three interpenetrating face centered cubic (fcc) lattices of Mn, Pt and Sn atoms. The Sn atoms locate at the centers of cubes formed by Mn and Pt atoms, but only half of atomic positions are occupied. Based on Rietveld refinement, the fitted lattice parameter is $a_{\rm sc} = 6.2964(1)$ Å, larger than the reported value of MnPtSn polycrystal ($a_{\rm poly} = 6.264$ Å).[25] In order to understand the origin of such a difference, the atomic ratio of MnPtSn single crystal was measured using the ICP-AES technique and the determined ratio of Mn : Pt : Sn is 0.446 : 0.616 : 1 when setting the content of Sn as 1. There are significant deviations from stoichiometry, possibly due to the anti-site defects caused by the excess of Sn occupying Mn and Pt sublattice sites. If assuming the occupation fraction of Sn atoms at Mn and Pt sites is x and y, respectively, the atomic ratio of Mn, Pt and Sn can be written as $1-x : 1-y : 1+x+y = 0.446 : 0.616 : 1$. The determined x and y are 0.351 and 0.104. Taking the reported atom radii $r_{\rm Mn} = 1.40$ Å, $r_{\rm Pt} = 1.35$ Å and $r_{\rm Sn} = 1.45$ Å,[26] the calculated unit cell parameter of stoichiometric MnPtSn is $a_{\rm cal} \approx 2(r_{\rm Mn} + r_{\rm Pt} + 2r_{\rm Sn})/\sqrt{3} = 6.524$ Å when assuming the close-packed arrangement to be along the [111] direction. If the Vegard's law is valid, the corresponding unit cell parameter with anti-site defects is $a_{\rm cal,defects} \approx 2[(1-x)r_{\rm Mn}+(1-y)r_{\rm Pt}+(2+x+y)r_{\rm Sn}]/\sqrt{3} = 6.557$ Å. Using the ratio of $a_{\rm cal,defects}/a_{\rm cal}$ and $a_{\rm poly}$, the evaluated $a_{\rm sc,cal}$ ($= a_{\rm cal,defects}/a_{\rm cal} \times a_{\rm poly}$) is 6.295 Å, very close to $a_{\rm sc}$. Thus, the increased lattice parameter of MnPtSn single crystal can be partially ascribed to the effect of Sn anti-site defects. Figure 1(c) exhibits the XRD pattern of a MnPtSn single crystal, indicating that the surface of the crystal is the (111) plane.

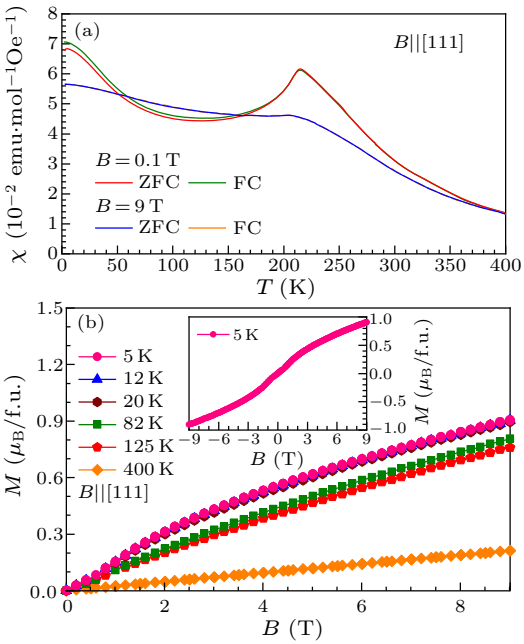

Fig. 2. (a) Temperature dependence of magnetic susceptibility $\chi(T)$ for MnPtSn single crystal with ZFC and FC modes at $B = 0.1$ T and 9 T for $B\|[111]$. (b) Isothermal magnetization $M(B)$ as a function of magnetic field B at various temperatures for $B\|[111]$. Inset: $M(B)$ loop from −9 to 9 T at 5 K.

Figure 2(a) shows the magnetic susceptibility $\chi(T)$ with zero-field-cooling (ZFC) and field-cooling (FC) modes at magnetic field $B = 0.1$ T and 9 T for $B\|[111]$. It clearly shows an antiferromagnetic transition at about $T_{\rm N} \sim 215$ K under a magnetic field of $B = 0.1$ T, in sharp contrast to the ferromagnetic transition $T_{\rm C}$ at 330 K for MnPtSn polycrystal.[20] At low temperature (∼125 K), the $\chi(T)$ curves show an

upturn behavior, implying that there may be a ferromagnetic interaction appearing. However, the almost overlapped ZFC and FC $\chi(T)$ curves at $B = 0.1$ T rule out the existence of magnetic glassy state in MnPtSn single crystal. Previous studies indicate that the arrangement of Mn atoms in IrMnGa has a critical influence on magnetic properties because the interaction of Mn local moments is highly sensitive to their distance, a consequence of the oscillatory Ruderman–Kittel–Kasuya–Yoshida (RKKY) exchange.[27] The anti-site disorder between Mn and Sn as well as Pt and Sn could lead to a randomly varying distance of the nearest and next-nearest neighbors of Mn atoms. Therefore, the competition between AFM and FM exchange interactions is expected.[27] It explains the distinct difference of magnetic properties between polycrystal and single crystal MnPtSn. Such a phenomenon has also been observed in Ni_2MnAl where the weak FM coupling appears in the ordered phase but it evolves into the AFM interaction once the disorder between Mn and Al sites becomes significant.[28] On the other hand, when the lattice shrinks with lowering temperature, the FM interaction may become stronger and start to affect the physical properties of MnPtSn. The T_N shifts to lower temperature and the cusp becomes smaller at $B = 9$ T, indicating that the AFM transition is suppressed by the high magnetic field. Figure 2(b) exhibits the isothermal magnetization $M(B)$ curves up to $B = 9$ T at various temperatures for $B\|[111]$. When $T < T_N$, the $M(B)$ curve shows a convex shape and it increases smoothly with field, but still does not saturate even in field up to 9 T. In addition, the $M(B)$ loop at 5 K (inset of Fig. 2(b)) does not exhibit any hysteresis behavior, confirming the AFM state below T_N. In contrast, the $M(B)$ increases linearly with field at 400 K, consistent with the paramagnetic state when $T > T_N$.

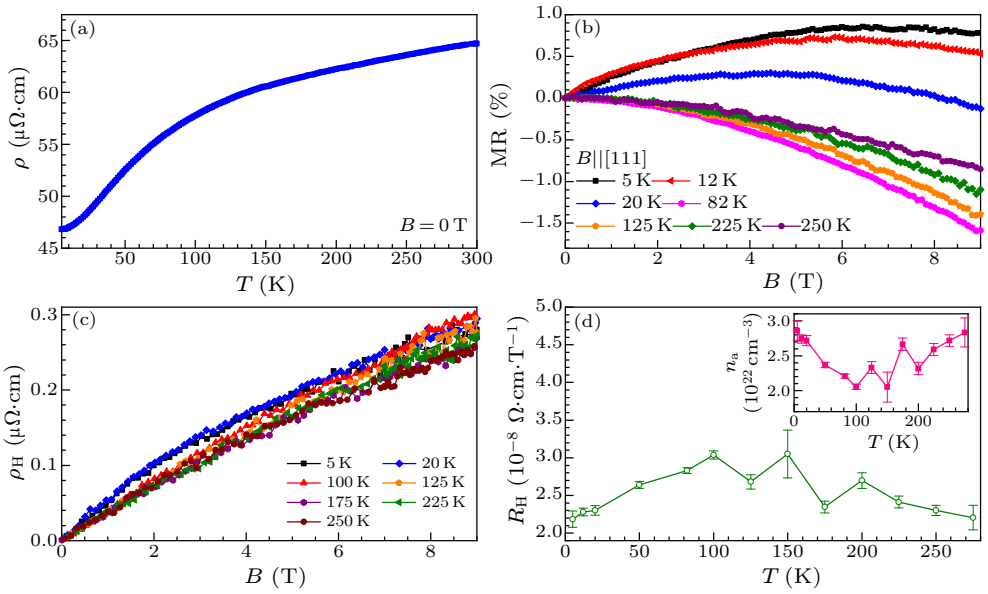

Fig. 3. (a) Temperature dependence of longitudinal resistivity $\rho(T)$ at zero field. (b) Field dependence of magnetoresistance MR at various temperatures for $B\|[111]$. (c) Hall resistivity $\rho_H(B)$ as a function of B at various temperatures for $B\|[111]$. (d) Temperature dependence of Hall coefficient $R_H(T)$ derived from $\rho_H(B)$. Inset: temperature dependence of apparent carrier concentration $n_a(T)$.

Longitudinal resistivity $\rho(T)$ as a function of temperature at zero field for MnPtSn single crystal is shown in Fig. 3(a). It shows a typical metallic behavior. Moreover, the absence of kink near T_N in the $\rho(T)$ curve suggests the relatively weak magnetic scattering in AFM MnPtSn. On the other hand, the $\rho(T)$ curve decreases quickly when $T <\sim 125$ K, implying that the possible FM interaction suppresses the magnetic scattering. Figure 3(b) represents the B-field dependence of magnetoresistance $[\mathrm{MR} = (\rho(T,B) - \rho(T,0))/\rho(T,0) \times 100\%)]$ at various temperatures for $B\|[111]$. At low temperature ($T \leq 20$ K), the MR increases with field at the beginning and then starts to decrease at higher field. The maximum value of MR at 5 K reaches ~0.85% at $B = 6.4$ T. The maximum positive value of MR and the corresponding field decrease gradually with increasing temperature. At higher temperature ($T \geq 82$ K), the MR becomes negative in the whole field range even above T_N, whereas the absolute value of MR decreases monotonically with increasing temperature. The positive MR at low temperature and low field could originate from the effect of Lorenz force. In contrast, the negative MR may arise from the suppression of magnetic scattering. Such behavior is most obvious near the temperature where the FM interaction just emerges. The smaller nega-

tive MR at higher temperature could be related to the increasing $\rho(T,0)$ due to enhanced electron-phonon scattering. Hall resistivity $\rho_{\rm H}(B)$ as a function of B at various temperatures is shown in Fig. 3(c). The $\rho_{\rm H}(B)$ curves are almost linear at high temperatures and slightly bend at low temperatures in low-field region. The ordinary Hall coefficient $R_{\rm H}$ can be determined from the slope of the linear fit of $\rho_{\rm H}(B)$ curve in high field region ($B > 5$ T). The obtained $R_{\rm H}$ as a function of temperature is shown in Fig. 3(d). The $R_{\rm H}$ is positive from 5 K to 275 K, indicating that the hole carriers are dominant. When compared to stoichiometric MnPtSn polycrystal which is a ferromagnet,[20] the absence of AHE further confirms the AFM ground state in the present MnPtSn single crystal. As shown in the inset of Fig. 3(d), the estimated apparent carrier concentration $n_{\rm a}(T)$ ($= 1/|e|R_{\rm H}$ with the elementary charge e) at 5 K is about 2.86×10^{22} cm^{-3}. Moreover, the $n_{\rm a}$ shows a weak temperature dependence (∼2.05–2.86×10^{22} cm^{-3}), implying that the single band model should be valid and the Fermi surface is insensitive to temperature in MnPtSn. It has to be noted that the $n_{\rm a}$ shows a minimum near 125 K, suggesting that the emergence of FM interaction could have some influence on electronic structure. The calculated mobility $\mu = R_{\rm H}/\rho(T,0)$ is 4.7 cm^2·V^{-1}s^{-1} at 5 K and such low carrier mobility can be partially ascribed to the significant disorder effect of anti-site defects in MnPtSn single crystal.

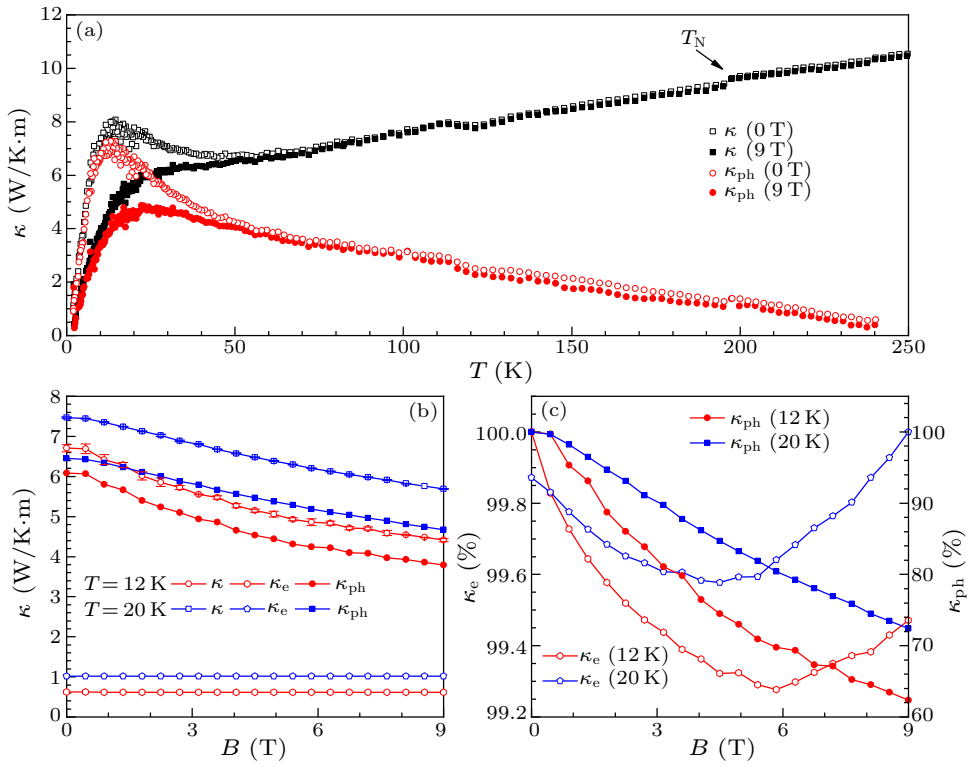

Fig. 4. (a) Temperature dependence of thermal conductivity $\kappa(T)$ at $B = 0$ T and 9 T. (b) Field dependence of $\kappa(B)$, electron thermal conductivity $\kappa_{\rm e}(B)$ and phonon thermal conductivity $\kappa_{\rm ph}(B)$ at various temperatures for $B\|[111]$. (c) Field dependence of normalized $\kappa_{\rm e}(B)$ and $\kappa_{\rm ph}(B)$ at various temperatures.

Figure 4(a) shows the temperature dependence of thermal conductivity $\kappa(T)$ under 0 T and 9 T with $B\|[111]$. It shows a jump near $T_{\rm N}$. Moreover, the $\kappa(T)$ shows a peak at low temperature (∼14 K) and it is suppressed dramatically by magnetic field. In fact, κ is composed by phonon thermal conductivity $\kappa_{\rm ph}$ and electron thermal conductivity $\kappa_{\rm e}$, i.e., $\kappa = \kappa_{\rm ph} + \kappa_{\rm e}$. The $\kappa_{\rm e}$ can be calculated by the Wiedemann–Franz law with the form $\kappa_{\rm e} = L_0\sigma T$ where $L_0 = 2.44 \times 10^{-8}$ W·Ω·K^{-2} is the Lorentz number and σ is the electric conductivity. Then the $\kappa_{\rm ph}$ can be extracted from the $\kappa - \kappa_{\rm e}$, as shown in Fig. 4(a). The $\kappa_{\rm ph}(T)$ still exhibits a jump near the $T_{\rm N}$, implying that the change of magnetic order will affect the phonon scattering. There is another kink around 125 K, which could also be related to the increased FM interaction at low temperature. At low temperature, there is still a big difference between zero-field $\kappa_{\rm ph}$ and that at $B = 9$ T, similar to $\kappa(T)$. In order to study this behavior further, we measured the field dependence of $\kappa(B)$ near the peak position ($T = 12$ K and 20 K) (Fig. 4(b)). The error bars reflect the stan-

dard deviation of multiple measurements (5 times) at each field. Figure 4(b) also shows the field dependence of $\kappa_e(B)$ and $\kappa_{ph}(B)$ calculated from the MR results. It can be seen that at these two temperatures, the contribution of $\kappa_{ph}(B)$ is much larger than that of $\kappa_e(B)$ even though MnPtSn shows a metallic behavior. The similarity of $\kappa(B)$ and $\kappa_{ph}(B)$ suggests that the suppression of total thermal conductivity with field is mainly caused by the monotonic decrease of phonon part. The change of the normalized value of $\kappa^n_{ph}(B) = \kappa_{ph}(B)/\kappa_{ph}(0\,\mathrm{T})$ is huge, reaching ~40% and 30% at 9 T for $T = 12$ K and 20 K, respectively (Fig. 4(c)). Such behavior is very exotic because the κ_{ph} is usually insensitive to field. However, similar phenomenon has also been observed in some materials, such as geometric frustrated spin system[29,30] and high-T_C superconductor,[31] and this is explained by the interplay between the magnetic excited quasiparticles and heat carriers. Further study of magnetic structure as well as magnetic excitation spectrum is needed to verify this conjecture. In contrast, the $\kappa_e(B)$ decreases with field at low field but increases at high field (Fig. 4(c)). Also, the change is very small in the order of 1% at 12 K, which becomes even smaller at higher temperature (20 K). The small $\kappa_e(B)$ is partially ascribed to the relative low mobility of MnPtSn and the weak field dependence of $\kappa_e(B)$ originates from the small MR. These phenomena could be related to the existence of significant anti-site defects.

In summary, we have grown half-Heusler compound MnPtSn single crystals successfully using the Sn flux method. MnPtSn single crystal with expanded unit cell has an AFM transition at about 215 K. The linear Hall resistivity with positive slope indicates that the dominant carriers are hole-type and the AHE is absent, remarkably different from the stoichiometric FM MnPtSn polycrystal. Moreover, MnPtSn single crystal exhibits a strong field dependence of phonon thermal conductivity at low temperatures. The off-stoichiometry of Mn and related Mn/Sn anti-site defects could be crucial for the change of structural and physical properties.

References

[1] Wolf S A, Awschalom D D, Buhrman R A, Daughton J M, von Molnár S, Roukes M L, Chtchelkanova A Y and Treger D M 2001 *Science* **294** 1488

[2] Galanakis I and Dederichs P H 2005 *Half-metallic Alloys: Fundamentals and Applications* (Berlin: Springer-Verlag) p 1

[3] Katsnelson M I, Irkhin V Y, Chioncel L, Lichtenstein A I and de Groot R A 2008 *Rev. Mod. Phys.* **80** 315

[4] Hirohata A, Sagar J, Lari L, Fleet L R and Lazarov V K 2013 *Appl. Phys. A* **111** 423

[5] Hirohata A and Takanashi K 2014 *J. Phys. D* **47** 193001

[6] Felser C, Wollmann L, Chadov S, Fecher G H and Parkin S S P 2015 *APL Mater.* **3** 041518

[7] Geldart D J W and Ganguly P 1970 *Phys. Rev. B* **1** 3101

[8] Podgornykh S M, Streltsov S V, Kazantsev V A and Shreder E I 2007 *J. Magn. Magn. Mater.* **311** 530

[9] de Groot R A, Mueller F M, van Engen P G and Buschow K H J 1983 *Phys. Rev. Lett.* **50** 2024

[10] Ishida S, Fujii S, Kashiwagi S and Asano S 1995 *J. Phys. Soc. Jpn.* **64** 2152

[11] Galanakis I, Dederichs P H and Papanikolaou N 2002 *Phys. Rev. B* **66** 174429

[12] Graf T, Felser C and Parkin S S P 2011 *Prog. Solid State Chem.* **39** 1

[13] Jourdan M, Minár J, Braun J, Kronenberg A, Chadov S, Balke B, Gloskovskii A, Kolbe M, Elmers H J, Schönhense G, Ebert H, Felser C and Kläui M 2014 *Nat. Commun.* **5** 3974

[14] Jeong T, Weht R and Pickett W E 2005 *Phys. Rev. B* **71** 184103

[15] Singh S, DSouza S W, Nayak J, Suard E, Chapon L, Senyshyn A, Petricek V, Skourski Y, Nicklas M, Felser C and Chadov S 2016 *Nat. Commun.* **7** 12671

[16] Canfield P C, Thompson J D, Beyermann W P, Lacerda A, Hundley M F, Peterson E, Fisk Z and Ott H R 1991 *J. Appl. Phys.* **70** 5800

[17] Suzuki T, Chisnell R, Devarakonda A, Liu Y T, Feng W, Xiao D, Lynn J W and Checkelsky J G 2016 *Nat. Phys.* **12** 1119

[18] Shekhar C, Kumar N, Grinenko V, Singh S, Sarkar R, Luetkens H, Wu S, Zhang Y, Komarek A C, Kampert E, Skourski Y, Wosnitza J, Schnelle W, McCollam A, Zeitler U, Kübler J, Yan B, Klauss H H, Parkin S S P and Felser C 2018 *Proc. Natl. Acad. Sci. USA* **115** 9140

[19] Singha R, Roy S, Pariari A, Satpati B and Mandal P 2019 *Phys. Rev. B* **99** 035110

[20] Otto M J, Feil H, van Woerden R A M, Wijngaard J, van der Valk P J, van Bruggen C F and Haas C 1987 *J. Magn. Magn. Mater.* **70** 33

[21] Li Y, Ding B, Wang X, Zhang H, Wang W and Liu Z 2018 *Appl. Phys. Lett.* **113** 062406

[22] Swekis P, Markou A, Kriegner D, Gayles J, Schlitz R, Schnelle W, Goennenwein S T B and Felser C 2019 *Phys. Rev. Mater.* **3** 013001(R)

[23] Vir P, Gayles J, Sukhanov A S, Kumar N, Damay F, Sun Y, Kübler J, Shekhar C and Felser C 2019 *Phys. Rev. B* **99** 140406(R)

[24] Liu Z H, Burigu A, Zhang Y J, Jafri H M, Ma X Q, Liu E K, Wang W H and Wu G H 2018 *Scr. Mater.* **143** 122

[25] Buschow K H J, van Engen P G and Jongebreur R 1983 *J. Magn. Magn. Mater.* **38** 1

[26] Slater J C 1964 *J. Chem. Phys.* **41** 3199

[27] Kroder J, Manna K, Kriegner D, Sukhanov A S, Liu E K, Borrmann H, Hoser A, Gooth J, Schnelle W, Inosov D S, Fecher G H and Felser C 2019 *Phys. Rev. B* **99** 174410

[28] Simon E, Vida J G, Khmelevskyi S and Szunyogh L 2015 *Phys. Rev. B* **92** 054438

[29] Jeon B, Koteswararao B, Park C B, Shu G J, Riggs S C, Moon E G, Chung S B, Chou F C and Kim K H 2016 *Sci. Rep.* **6** 36970

[30] Sharma P A, Ahn J S, Hur N, Park S, Kim S B, Lee S, Park J G, Guha S and Cheong S W 2004 *Phys. Rev. Lett.* **93** 177202

[31] Peacor S D, Cohn J L and Uher C 1991 *Phys. Rev. B* **43** 8721